Chapter III

Materials and Experimental Procedure

This chapter provides detailed information about the procedures involved in synthesis of wurtzite(wz) $Cu(In_xGa_{1-x})S_2$ NPs and ink preparation, deposition of wz-$CuInS_2$ ink, selenization of $CuInS_2$ film, chemical bath deposition of CdS, RF sputtering of window layer deposition, thermal evaporation for front contact deposition. A brief description of the utilized characterization techniques and analytical methods including X-ray diffraction, electron microscopy and spectroscopy techniques is presented in this chapter. The working principles of the characterization techniques are discussed.

III.1 Materials

Copper (II) acetylacetonate ($C_{10}H_{16}CuO_4$,,≥99.99%) Cu(acac), Indium (III) acetylacetonate ($C_{15}H_{21}InO_6$,≥ 99.99%) In(acac), Gallium (III) acetylacetonate ($C_{15}H_{21}GaO_6$, ≥99.99%) Ga(acac), Trioctylphosphine oxide ($OP(C_8H_{17})_3$) (TOPO), Oleylamine ($C_{18}H_{37}N$, 70%) (OAm), 1-dodecanethiol ($C_{12}H_{26}S$, 98%) (1-DDT), tert-dodecanethiol ($C_{12}H_{26}S$, 98.5%) (t-DDT), Selenium shots (Se, 99.99%) cadmium acetate hydrate ($Cd(CH_3COO)_2$, ≥99.99%), thiourea (CH_4N_2S, ≥ 99.0%) were purchased from Sigma Aldrich. NH_4OH (25% GR, Merck), Hexane (C_6H_{14}) and ethanol (C_2H_6O) were purchased from Merck. All the precursors were used as

received, without any further purification. The molybdenum coated soda-lime glass was procured from Techinstro, India.

III.2 Synthesis of wz-Cu(In_xGa_{1-x})S_2 NPs and Ink Preparation

In the present work, the nanoparticle-ink-based solution processing approach has been adopted. The synthesis of wz-Cu(In_xGa_{1-x})S_2 (x= 0, 0.3, 0.5, 0.7, 1) NPs by hot injection method was carried out in an inert atmosphere using a Schlenk set-up.

III.2.1 Hot Injection Method

The present approach to synthesize monodisperse NPs is predominantly based on the work of LaMer and Dinegar [165]. They described how the formation of monodisperse colloidal NPs is reliant on fast nucleation followed by the controlled growth of the existing nuclei. Peng *et al.* and Murray *et al.* [166, 167] introduced the "hot-injection" method for the synthesis of monodisperse CdS, CdSe, and CdTe QDs. The method involves the formation of homogeneous nuclei via the rapid injection of organometallic reagents into a hot solvent. The reaction solution used during this process also contains surfactant (trioctylphosphine oxide (TOPO), oleylamine (OAm), etc.) ligands to prevent NPs from agglomerating.

III.2.2 Schlenk Line Set-up

Schlenk line set-up enables the synthesis of air-sensitive materials as the reactions can be performed under a vacuum or inert gas atmosphere. This set-up was first designed and established by "Wilhelm Schlenk". A schematic and experimental setup of the schlenk line setup utilized in this work is depicted in **Figure III.1(a)** and **(b)**, respectively. The Schlenk lines are switchable dual manifolds, where one

line is associated with an inert gas (argon or nitrogen) and the other line is connected to a vacuum pump. The nitrogen flows out through an oil bubbler, which allows a slight overpressure of nitrogen inside the round bottom flask (RBF) and monitoring of the gas flow. A 100 ml three-necked RBF is connected to the manifolds via silicon tubing and two way switch valves which allow switching between pumping and purging without exposing to the atmosphere. Additional apparatus contains a rubber stopper that a syringe can perforate, a thermometer immersed in the reaction mixture, a condenser, and a rotamantle to heat the RBF. Schlenk line set-up has been used for the synthesis of nanosheets and nanoparticles of a diverse class of sulphide and selenide compounds including ZrS_2 [168], TiS_2, HfS_2 [169], $MoSe_2$, WSe_2 [170], CIS[171], CIGS[172], and CZTS [41].

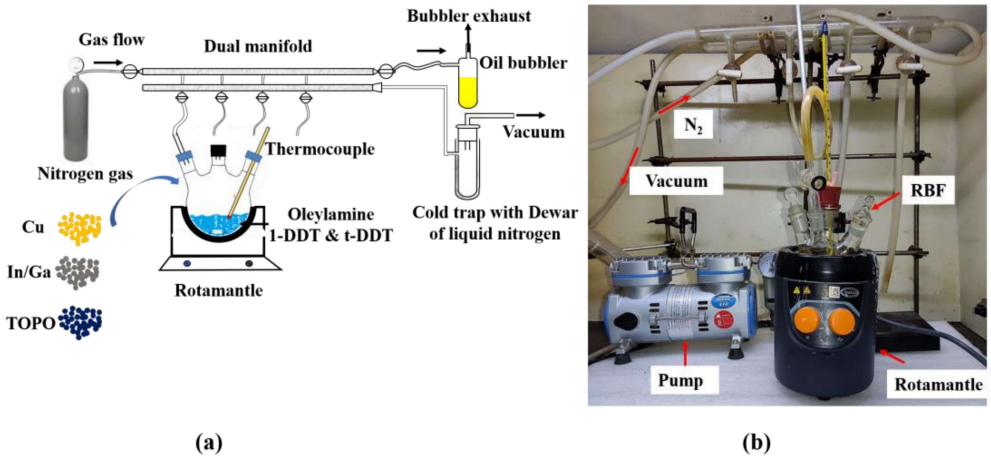

Figure III.1 (a) Schematic representation and (b) experimental setup of Schlenk line for the synthesis of wz-Cu(In_xGa_{1-x})S_2 nanoparticles.

III.2.3 Synthesis of wz-Cu(In_xGa_{1-x})S_2 NPs

The synthesis of wz-Cu(In_xGa_{1-x})S_2 NPs was carried out using the hot injection technique. A schematic flowchart of the synthesis method is depicted in **Figure III.2**. Synthesis was carried out in a round-bottom flask (RBF) in a nitrogen atmosphere. Metal-(acac) precursors of copper (1 mmol) and indium/gallium (1 mmol) are mixed with the TOPO (3.5 mmol) and OAm (10 ml) in an RBF. The RBF was evacuated and purged with nitrogen gas. This process was repeated three to four times to ensure the degassing of the solution. The reaction mixture was slowly heated up to 160 °C. On heating to 50 °C, the transparent blue solution formed **(Figure III.2(bottom))**. On heating, the solution turned light green indicating the formation of a copper complex with OAm and TOPO (~100 °C), and on heating to ~150°C the color changes to dark green due to the formation of an indium complex. A mixture of 1-DDT (0.25ml) and t-DDT (1.75ml) (sulfur source) was prepared separately. The prepared 1-DDT and t-DDT solution mixture were rapidly injected (hot injection) into the metal precursor solution at 160 °C under continuous stirring (100 rpm). The solution turned essentially clear with a light yellow tint with no sign of any precipitation **(Figure III.2)**, indicating to the formation of metal ions due to the decomposition of metal complexes. After adding the sulfur source, the temperature was increased, at the rate of ~6 °C/min, up to 310 °C and was held at that temperature for about 1 h. After one hour the sample was allowed to cool down to room temperature. The NPs were separated out from the solution by several cycles of centrifuging and washing. Ethanol and hexane were used for washing. The color of the obtained final product varied from black for $CuInS_2$, dark red for $CuIn_{0.5}Ga_{0.5}S_2$, to dark yellow for $CuGaS_2$. The chemical

reaction during synthesis of wz-CIS nanoparticles through formation of copper sulfide and indium sulfide as follows:

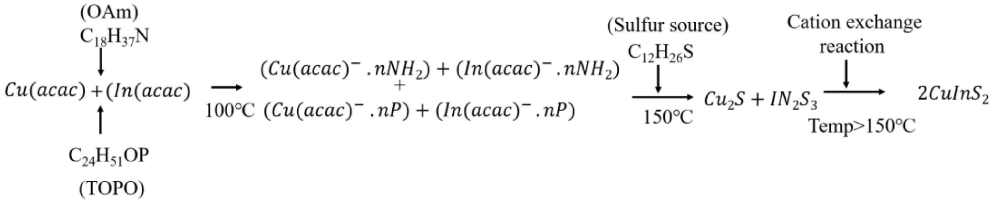

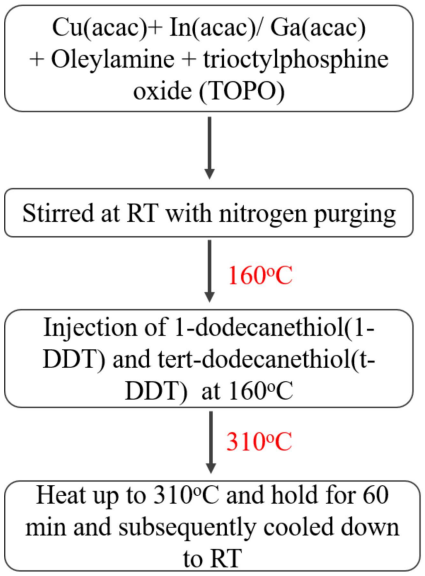

Figure III.2 Flowchart of producing $Cu(In_xGa_{1-x})S_2$ NPs from metal precursor through the hot-injection method and color change observed during reaction with respect to temperature.

III.2.4 Nanoparticle Ink Formation

$Cu(In_xGa_{1-x})S_2$ NPs can be dispersed in toluene as solvents and 1-dodecanethiol as stabilizing ligands in the ratio of 45:1 to form an ink. Toluene has a low boiling point of 110 ^oC, which can easily evaporate. To ensure excess sulfur environment to form the p-type absorber layer 1-dodecanethiol is used. Important aspect considered for the ink formulation included: (1) long-term nanoparticle stability in the solvent to avoid clogging, (2) appropriate fluid properties for formation of a stable drop generation, (3) good substrate wetting, and (4) suitable solvent evaporation rate to avoid the formation of cracks and pin holes [173].

The formulated inks were coated on soda-lime glass/molybdenum-coated soda-lime glass by spray coating using nitrogen as a carrier gas under ambient conditions.

III.3 Spray Coating

The $Cu(In_xGa_{1-x})S_2$ films were spray deposited utilizing a commercial spray pyrolysis system purchased from Holmarc Opto-mechatronics Pvt. Ltd., India. A schematic and a picture of the spray pyrolysis setup are shown in **Figure III.3(a) and (b) respectively**. The $Cu(In_xGa_{1-x})S_2$ film was fabricated by spraying the CIS NPs of 260g suspension in a 90 ml of dispersant mixture (toluene and 1-DDT in 45:1 ratio) onto heated substrates at 250 °C in an ambient condition using nitrogen as carrier gas. The spray rate was controlled by a syringe pump (Unigenetics Instruments Pvt. Ltd., India). The speed of the spray nozzle was set as 300 mm/s in the *x*-direction and 6 mm/s in the *y*-direction while the precursor flow rate was 2 ml/min and the distance between the substrate and spray head nozzle was kept at ~12 cm. The nozzle pressure was adjusted to about 1 bar.

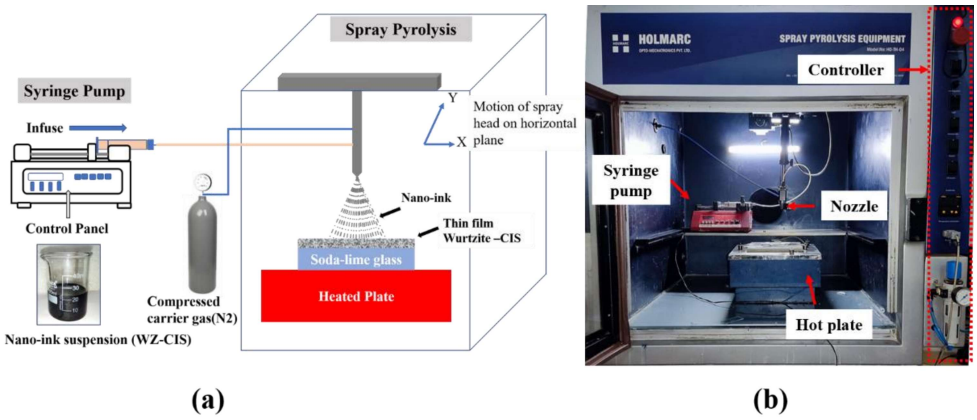

Figure III.3 (a) Schematic representation and (b) a picture of the spray pyrolysis system utilized for the deposition of wz-Cu(In_xGa_{1-x})S_2 film.

III.4 Selenization

Selenization is the process where a film is exposed to a selenium containing atmosphere at a high temperature. The film reacts and forms a new compound on incorporating selenium. In this case, the selenization was carried out to partially substitute the Se for S in Cu(In_xGa_{1-x})S_2. The selenization is known to result in grain growth, defect/grain boundary passivation and bandgap tuning. Formation of a thin layer of $MoSe_2$ at CIGS/Mo interface is also believed to improve adhesion between absorber layer. A schematic and a picture of selenization setup are shown in **Figure III.4(a)** and **(b)**, respectively. The as-deposited wz-Cu(In_xGa_{1-x})S_2 thin films together with selenium shots were placed into a covered graphite box. The box was placed in a tubular furnace (Ants Ceramic Pvt. Ltd, India, **Figure III.4(c)**) and was heated under the flowing argon gas. The argon flow rate was controlled using a mass flow controller (Bronkhorst, Netherland). Before selenization the tube furnace was purged with Ar gas at 120 °C to remove any adsorbed moisture or oxygen from sample and tube furnacesusing vacuum pump. After pumping and purging several

times, the tube was filled with argon gas and flow rate was set at 20 sccm (standard cubic centimeters per minute) using mass flow controller. Temperature profile of the tubular furnace during selenization is shown in **Figure III.4(d)**.

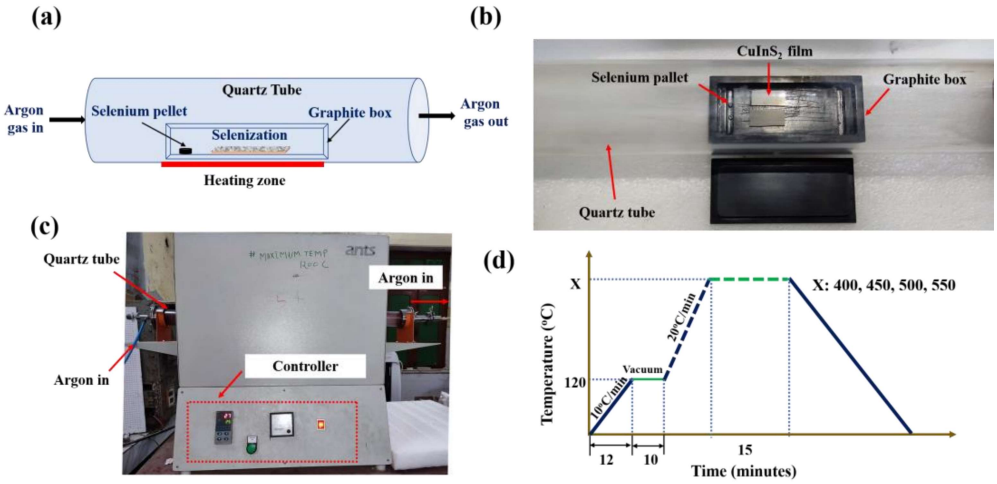

Figure III.4 (a) Schematic diagram of selenization set-up with flowing argon gas, (b) Experimental set-up with graphite box containing selenium shots and wz-CIS film, (c) Photograph of high temperature tube furnace, (d) Temperature profile for the selenization process.

Selenization was carried out at temperature varying from 400 to 550 °C for up to 15 mins, while the ramp rate was fixed at 20 °C/min. Subsequently, the tube furnace **(Figure III.4(c))** was allowed to cool naturally with a constant flow of argon. A part of selenium vapor can also come out long with the flowing argon which is toxic. In order to trap the selenium vapour and stop it from being released into the atmosphere, the out flowing gas was bubbled through a bleach solution.

III.5 Chemical Bath Deposition

Chemical bath deposition (CBD) is a widely used technique for sulfide thin films deposition. The coating is obtained by dipping stationary substrates in a stirred chemical bath. The chemical bath contains the chalcogenide source, the metal ion and a complexing agent that modify the pH. In CBD process, the film thickness and chemical composition are easily controlled by varying the deposition parameters such as temperature, precursor concentration, pH and time. CBD being scalable, cheaper and its requirement of very low annealing temperature are its major attractive aspects.

The CdS thin layer was deposited on soda-lime glass and selenized $Cu(In_xGa_{1-x})(S, Se)_2$ (for device fabrication) film by the CBD method. A flowchart of the formation CdS thin film processing is shown in **Figure III.6** .

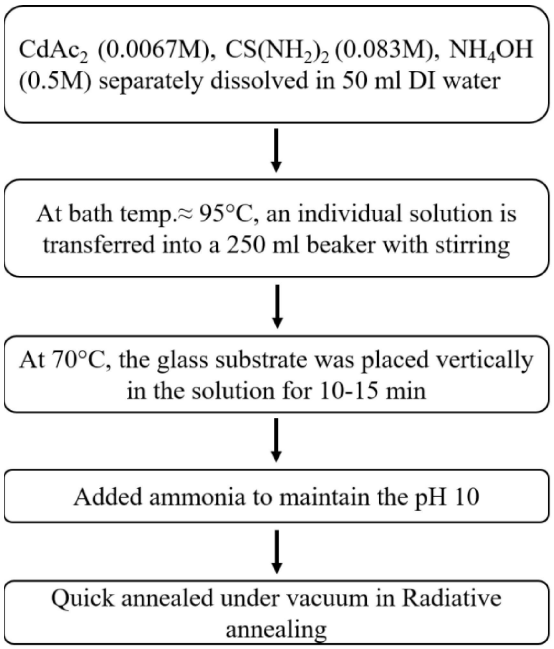

Figure III.5 Flowchart of formation CdS thin film through fast annealing process

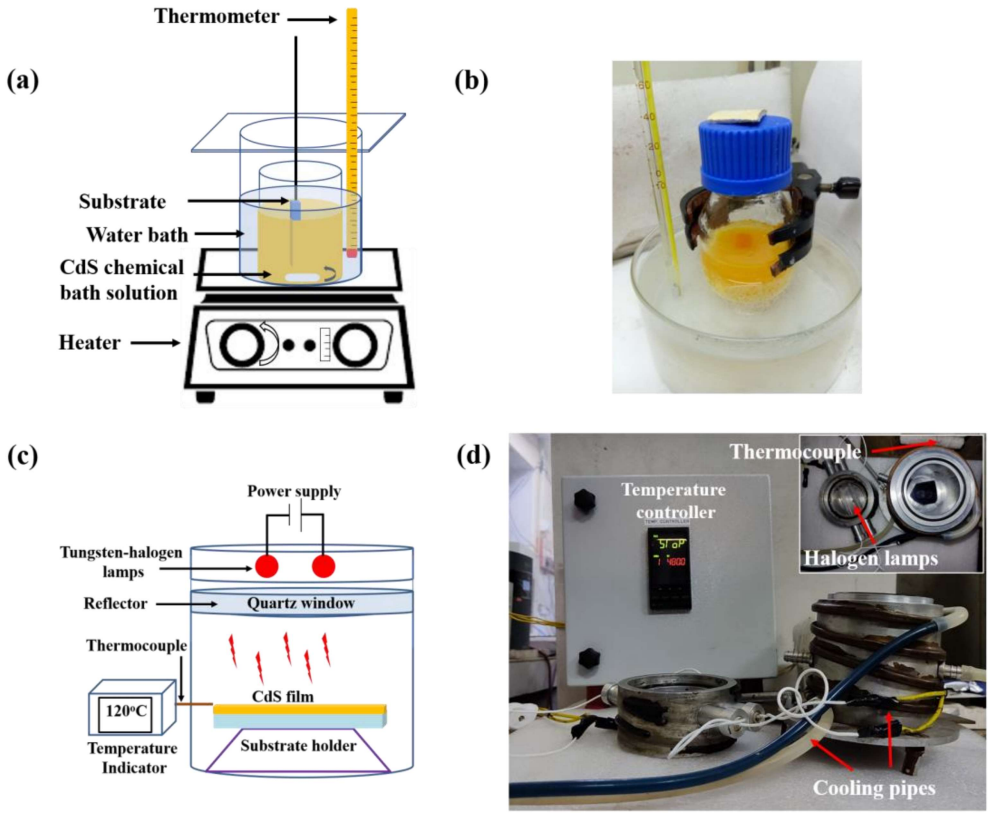

Figure III.6 (a) Schematic and (b) Picture setup of chemical bath deposition, (c) Schematic and (d) Photograph setup of radiative annealing of CdS layer.

The CdS buffer layer is fabricated by CBD at 70 °C using a solution containing $Cd(CH_3CO_2)_2$ as cadmium source, thiourea ($SC(NH_2)_2$) as sulfur precursor, ammonium (NH_4OH) as complexing agent. A schematic and a picture of CBD setup are shown in **Figure III.6(a)** and **(b)**, respectively. The substrate was dipped in the chemical bath for 15 mins and afterward was rinsed with DI water. The films were annealed in a radiative annealing setup (**Figure III.6 (c)** and **(d)**) for 5 minutes at 120°C. In the beginning of the film deposition, the growth was mainly governed by the ion-by-ion growth mechanism, then the cluster-by-cluster mechanism turned out to be dominant (details discussed in chapter VII).

III.6 Radio Frequency Sputtering

Sputtering is a high-vacuum thin film deposition technique by the material removal from a solid surface as a consequence of momentum transfer between an energetic particle, usually an ion, and the surface. These energetic particles originate from the continuous current glow discharge, which is created by applying a voltage between the target (cathode) and substrate (anode) electrodes in the presence of an argon gas kept at low pressure inside a sputtering chamber. The applied voltage accelerates the electrons towards the anode and while the electrons are accelerated, they collide with the gas atoms and the cascading effect of collision ionizes the gas. The positively charged (Ar^{+}) ions are now accelerated towards the cathode(-ve), causing a high energy impact on the target surface and the emission of secondary electrons. Further, these electrons can be accelerated towards the anode and generate new collisions (causing a cascade effect) creating a stable discharge, and keeping the plasma in an equilibrium condition. For the ejection of an atom from the surface of the target a series of collisions with positive ion is required, usually, it takes two or more collisions and that atom has enough kinetic energy to reach the surface of the substrate.

Radio Frequency (RF) Sputtering is used for insulator targets, One of the fundamental reasons for using RF sputtering for non-conducting targets is that the glow discharge will not be sustained due to the immediate formation of a positively charged surface on the exposed face of the insulator material. Therefore, for maintaining the glow discharge using a non-conducting target, the DC power supply has to be replaced by an RF power supply. A schematic and a picture of the thin film deposition by RF sputtering are shown in **Figure III.7(a)** and **(b)**

respectively. The ZnO, Al:ZnO films were deposited in an RF magnetron sputtering system.

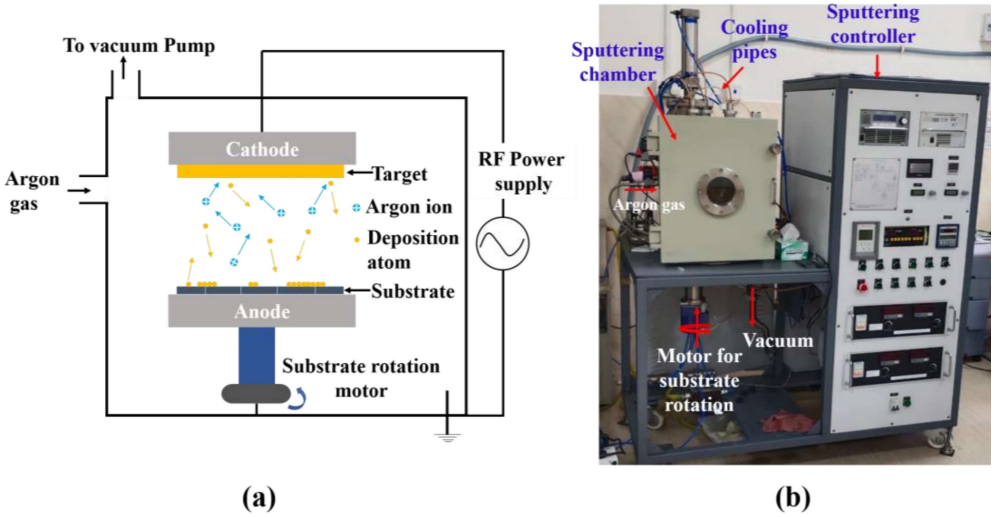

Figure III.7 (a) Schematic diagram and (b) Instrument photograph of RF magnetron sputtering system

The targets (50.4 mm diameter and 3 mm thickness) are mounted to the planar cathode and are held at a close range from the rotating substrate which serves as the anode surface. The processing chamber is then pumped down to the base pressure of 5x 10^{-6} mbar utilizing a rotary and a turbo pump. For deposition, the argon flow rate (~15 sccm) and the working pressure (1.3x10^{-1} mbar) were adjusted to achieve a stable glow discharge. Prior to deposition, pre-sputtering was performed with the aim of cleaning the surface impurities of the ZnO, Al:ZnO targets. The distance between the substrate and target was 6 cm. ZnO was deposited for 25 min at RF power 100 W to achieve 50-70 nm thin film, while a thickness of 220-250 nm was obtained for Al:ZnO by depositing at RF power 200 W for 15min.

III.7 Thermal Evaporation

Thermal evaporation is a well established technique for deposition of thin electrode layers. The required material evaporates in a high vacuum due to high temperature heating, which enables the direct deposition of vapour molecules/atoms over the substrate on which the vapour phase again condenses as a thin film. Here, the gold (99.99%, Hind High Vacuum Company Private Limited, India) electrical front contact was deposited over the Al:ZnO layer by thermal evaporation. The gold electrode was deposited under the working chamber pressure of $5x10^{-5}$ mbar (sketched in **Figure III.8(a)** and the photograph is shown in **Figure III.8(b))**.

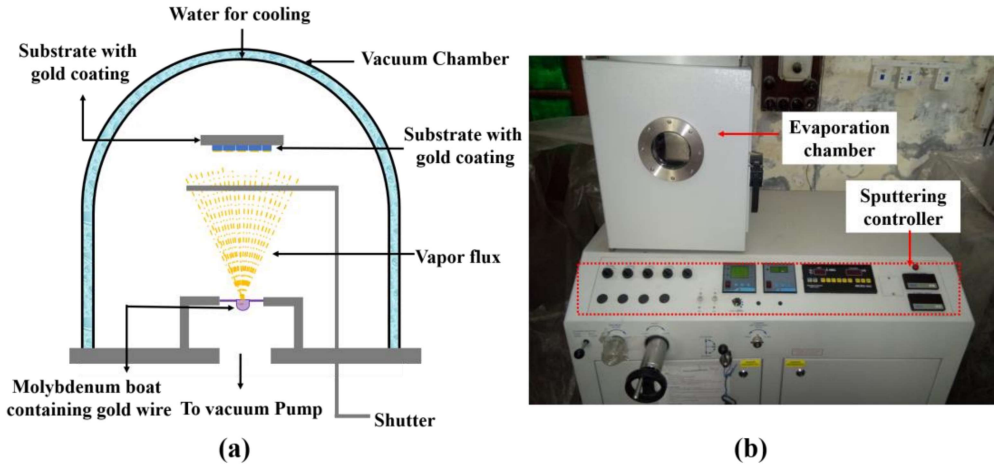

Figure III.8 (a) Schematic and (b) Photograph of the thermal evaporation system used for front contact in CIS device.

The processing chamber was evacuated initially using a roughing rotary pump up to 10^{-3} mbar, while high vacuum of the order of $5x10^{-5}$ mbar was achieved using a turbopump. A measured amount of Au wire (grade, Source) was placed in the molybdenum boat while 40-60 ampere current was supplied to vaporize the Au.

The thickness of the gold film was measured using digital thickness monitor while the mass of gold depended on the thickness.

III.8 Characterization Techniques

III.8.1 X-ray Diffraction and Grazing Incidence-XRD

X-ray Diffraction

XRD is the primary characterization tool used for crystallographic phase identification and phase quantification of materials. Diffraction peaks are generated when a beam of X-ray incident (of wavelength λ) on a crystalline material satisfies the Bragg condition i.e. $n\lambda = 2d_{(hkl)}Sin\theta$, where $2d_{(hkl)}$ is the interplanar spacing of *(hkl)* planes [174]. The X-ray diffraction patterns generated, deliver a unique "fingerprint" for crystallographic phase information. The X-ray diffraction patterns were recorded utilizing a diffractometer Rigaku Mini flex-600 (40 kV–15 mA); Rigaku, Tokyo, Japan using CuKα radiation (λ = 0.154060 nm). XRD data were recorded in the 2θ scan ranging from 20 to 70° at a step size of 0.02° with a scan rate of 2°/min. Line sketch of the conventional Bragg-Brentano geometry utilized for collecting XRD patterns and a picture of XRD instrument is shown in **Figure III.9(a)** and **(b)**. Relative intensity of the diffracted peaks was estimated for each diffracting plane using the relation:

$$I = |F|^2 P\left(\frac{1 + Cos^2\theta}{Sin^2\theta\ Cos\theta}\right)$$

Where, F is structure factor, P is multiplicity factor of the plane, $\left(\frac{1+Cos^2\theta}{Sin^2\theta\ Cos\theta}\right)$ is Lorentz-polarization factor Since all the patterns were recorded at room

temperature, the temperature factor was neglected. The structure factor (scattering from the atoms) for a unit cell from a given set of (hkl) planes is calculated from the summation of the amplitude function from each atom in the unit cell [uvw]:

$$F(hkl) = \sum_{n=1}^{N} f_n e^{2\pi i(hu+kv+lw)}$$

The width of the diffraction peaks carries information about the crystallographic domain size (equivalent to crystallite size) that can be calculated from the Scherrer's equation:

$$D = \frac{K * \lambda}{B * Cos\theta_B}$$

where, D= crystallite size, K= constant dependent on crystal shape (0.91 for spherical, 1 for elliptical) λ=X-ray wavelength, B=FWHM (full width at half maxima) or integral breadth, θ_B = Bragg angle.

Grazing Incidence X-ray Diffraction

Grazing Incidence X-ray Diffraction (GIXRD) is a surface sensitive diffraction technique that utilises a small incident angle X-ray beam to limit penetration and enhance the signal from films. The penetration depth can be estimated as a function of incidence angle omega(ω) as shown in **Figure III.9(c)**. The incident angle is kept constant while the detector collects the diffracted intensity through varying 2θ. thereby, keeping the X-ray foot print over the film constant throughout the experiment. The crystallographic phase of the CdS and window layer (i-ZnO and Al:ZnO) thin films were characterized by grazing incidence X-ray (Smart Lab,

Rigaku, Tokyo, Japan (**Figure III.9(d)**). The data were recorded at grazing incidence angle 0.3° (CdS), 0.5° (i-ZnO) and 1° (Al:ZnO) using CuKα radiation in the 2θ scan range from 20 to 70° at a step size of 0.02° and a scan rate of 2°/min.

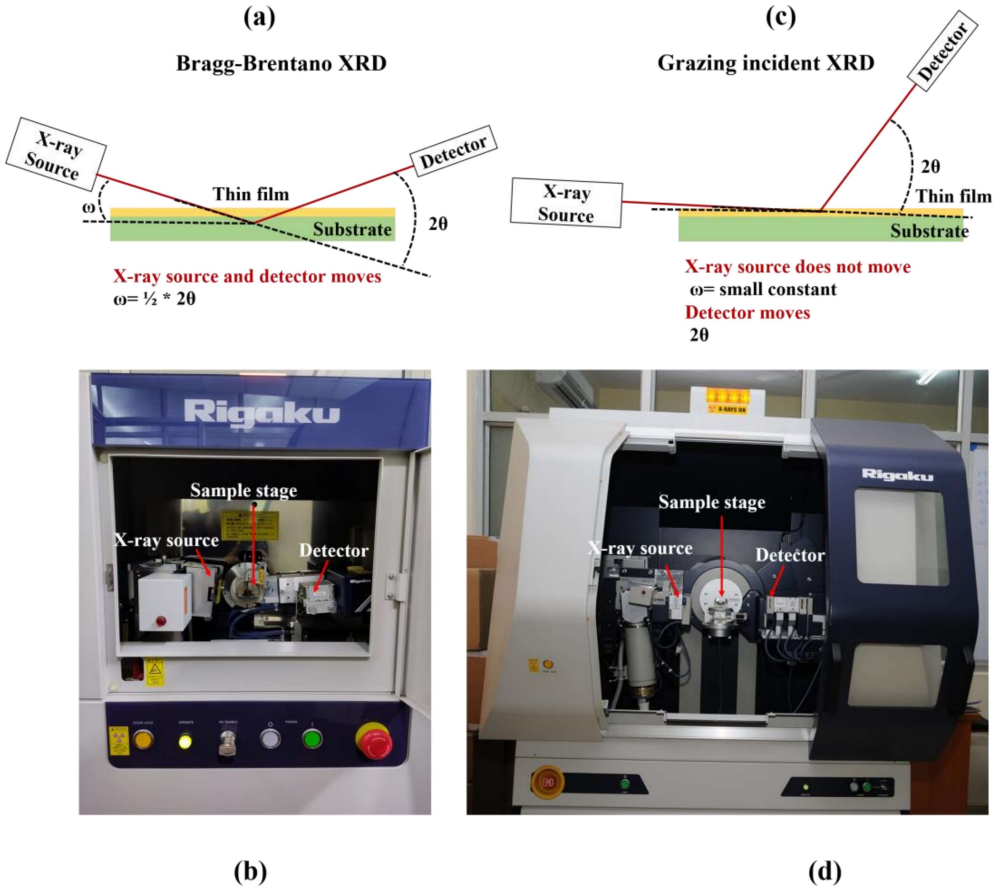

Figure III.9 (a) Bragg-Brentano geometry and (b) photograph of bench-top XRD, (c) Grazing incident geometry and (d) photograph of Grazing-Incidence XRD.

III.8.2 Field Emission Scanning Electron Microscopy

Field emission scanning electron microscopy (FESEM) is an advanced technology used to capture microstructure images for analysis of topographical and elemental information of the materials. FESEM consists of electron gun **(Figure III.10(a))** at

the top as source of electron beam with energy ranging from few hundred eV to few keV. The electrons are converged to form a fine probe of diameter < 5 nm through the electromagnetic lenses. The sample is scanned by rastering of electron beam over the sample surface using the scan coils. The high energy electrons penetrate the surface of the specimen and undergoes elastic and inelastic interactions **(Figure III.10(b))** generating a series of signals including secondary electron, backscattered electrons, characteristics X-rays and bremsstrahlung radiation. While secondary electrons are used for imaging surface topography, phase identification, and compositional contrast can be obtained from backscattered electrons. Energy dispersive X-ray spectroscopy (EDX) attached to FESEM is utilized to obtain elemental composition using the emitted characteristic X-rays **(Figure III.10(c))**.

The FESEM model Nova Nano SEM 450, supplied by FEI Company of USA (S.E.A.) PTE, LTD was utilized for imaging CIS, while the energy dispersive X-ray spectra of the CIS powders and film were acquired utilizing a customary unit (Pegasus Integrated EDS-EBSD with Octane Plus and Hikari Pro, EDAX Inc.) attached to the FESEM.

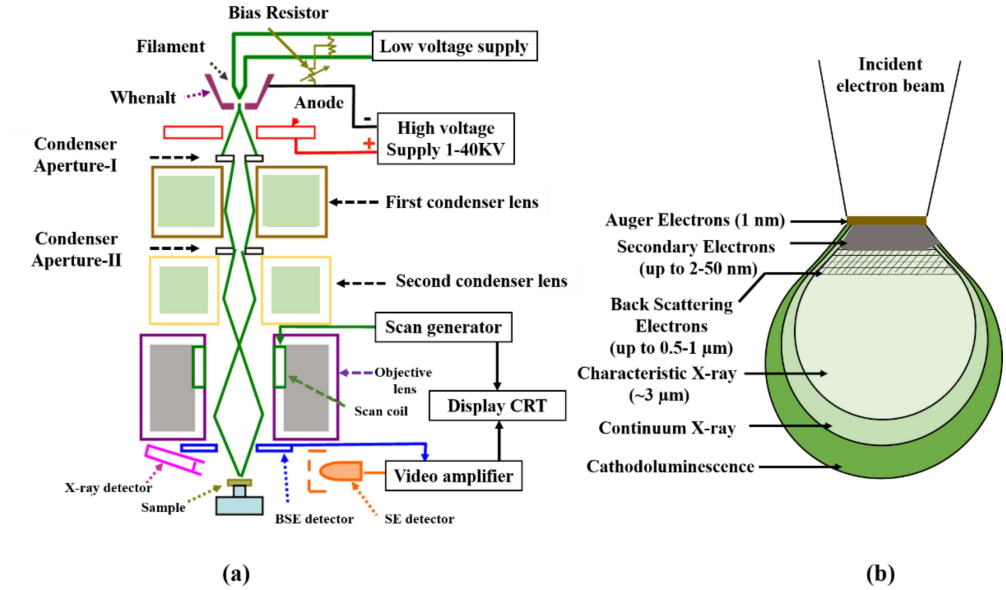

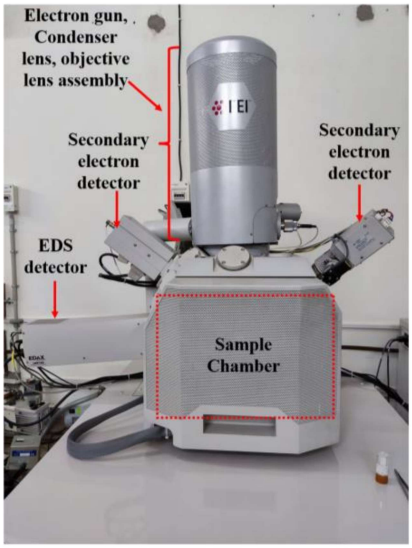

(c)

Figure III.10 (a) Schematic of SEM eliciting the incidence of electrons through various electromagnetic lenses, followed by scanning the sample surface and gathering the signals to generate the final image, (b) Interactions of electrons with matter in a scanning electron microscope with various signals, (c) Photograph of Field Emission Scanning Electron Microscope.

III.8.3 Transmission Electron Microscopy

Transmission electron microscopy (TEM) is a high-resolution technique used to reveal structural details, size distribution, and morphology of nanoparticles. In TEM, the high energy electron beam is accelerated at a voltage of ~ 200 kV and is transmitted through a thin specimen. The electron interact with the specimen as it passes through as shown in **Figure III.11(a)**. The resolution and magnification power of TEM are much greater than SEM. The resolving power of a microscope is governed by Rayleigh criteria, it shows that two-point objects are just resolvable if they are separated by the angle:

$$\theta = \frac{1.22\lambda}{D}$$

where 'λ' is the wavelength of the radiation and 'D' is aperture diameter. The wavelength of electron is calculated with the help of de Broglie's relationship:

$$\lambda = \left(\frac{h}{m * v}\right)$$

where *'h'* is the Plank's constant, *'v'* is the velocity of the electron and *'m'* is the mass of the electron. The wavelength of an electron accelerated at 200 kV is ~ 0.0025 nm as per de Broglie relationship.

In the present work, the TEM studies were carried out in a Tecnai G^2 T20 (*Cs* = 1.2 mm) TEM operated at 200 kV equipped with HAADF and STEM-EDS detectors. **Figure III.11(b)** shows the picture of complete cabinet. Only powder samples of $Cu(In_xGa_{1-x})(S,Se)_2$ were analysed to reveal the morphology, size and

distribution, and phase. Samples for TEM imaging were prepared by drop-casting NPs dispersed in ethanol onto a carbon-coated nickel (200-mesh) TEM grid.

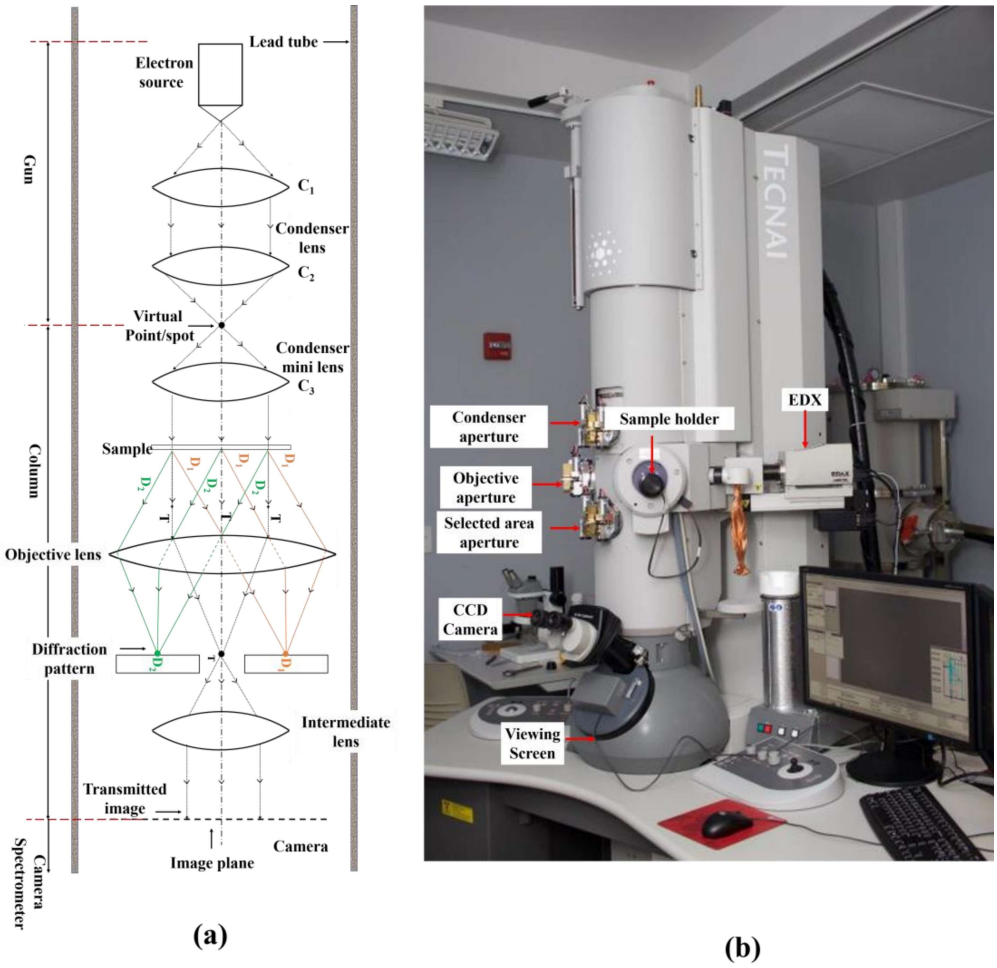

Figure III.11 (a) Schematic representing path of an electron beam in TEM, (b) Photograph of actual TEM machine with complete cabinet assembly.

The lattice interplanar spacing was estimated from the selected area electron diffraction pattern (SAED) using the relation, $r \times d = \lambda \times L$ (where, d= lattice spacings, λ= electron wavelength, r = relative space distance and L=camera length). Interplanar spacings obtained in this manner were used in conjunction with angles between diffraction spots to categorize phase in nanoparticles. Energy dispersive

X-ray spectroscopy is another function commonly used in conjunction with TEM. Signal was collected from areas of nanoparticle samples by use of limiting apertures. EDS was performed with a Tecnai G^2 T20, in STEM (scanning TEM) mode, to determine the local composition of both the monophasic and biphasic nanoparticles.

III.8.4 X-ray Photoelectron Spectroscopy

X-ray Photoelectron Spectroscopy (XPS) is a surface specific spectroscopy technique based on the photoelectric effect, which is generally used to find out the elemental composition, empirical formula, chemical state of the elements within a material by knocking out the electrons from the material using a focused X-ray beam. If photon energy(hv) is large enough, the core electron will then escape from the atom and emit out of the surface. **Figure III.12(a)** and **(b)** shows the schematic of the components of a typical photoelectron spectroscopy set-up and photoemission process used for XPS respectively. The binding energy of the ejected electrons can be expressed as $BE = hv - KE - \emptyset$, where hv is energy of the photon, KE is kinetic energy, and $\emptyset$ is work function that is defined as energy required to remove an electron from the Fermi edge of semiconductor material and is described as $\emptyset = E_{vac} - E_F$, where E_{vac} is vacuum energy and E_F is the Fermi energy of the material. The electron BE energy depends on the electronic configuration and is unique for each element and therefore enables elemental identification. A typical XPS spectrum is represented as number of electrons detected at a specific binding energy. The number of detected electrons in each peak is directly related to the amount of element within the XPS sampling volume, while any shift in peak position indicates to the changed chemical environment.

XPS was performed using PHI 5000 Versa Prob II (FEI Inc.) instrument; Mg Kα having a source energy of 1200 eV was used for the surface analysis using X-ray photoelectron spectroscopy. The pass energy of 2.95 eV and analyser work function was 4.105 eV, while C1s peak at the binding energy 284.8 eV was used as a reference. The surface of the specimen was sputter cleaned with Ar^+ ions (5 kV, 20 μA) prior to recording the XPS spectra.

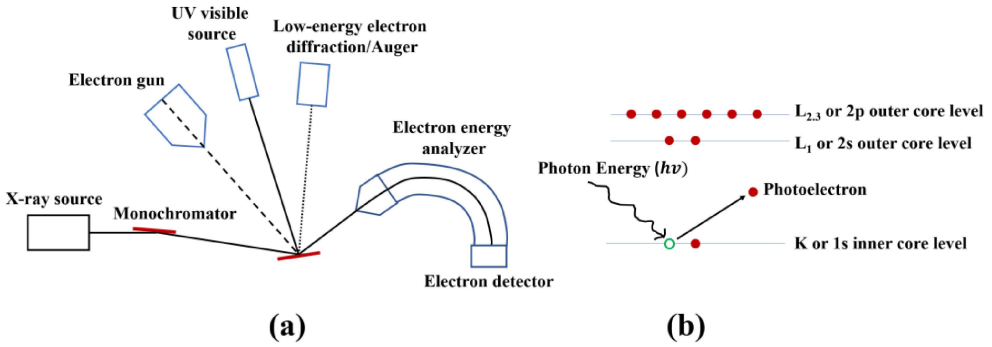

Figure III.12 Schematic diagram showing (a) the components of a typical photoelectron spectroscopy set-up, (b) photoemission process used for XPS.

III.8.5 Fourier Transform Infrared Spectroscopy

Fourier transform infrared spectroscopy (FTIR) is a preferred technique for infrared spectroscopy. FTIR was performed to find out intermediate compounds and the presence of functional groups on the surface of $Cu(In_xGa_{1-x})(S,Se)_2$ NPs by shining a beam containing many frequencies of light at once and measuring the frequency absorption. When color IR radiation is made to pass through a sample, some radiation is absorbed and some of it is transmitted by the sample. The resulting signal after absorption at sample is collected by a detector. The obtained spectrum represents a molecular 'fingerprint' of the sample. As shown in **Figure III.13 (a)** ,

a light from the infrared source is guided to the interferometer as a collimated beam, and split into two paths as transmitted and reflected beams. The two beams are reflected by the fixed mirror and the moving mirror, they return to the beam splitter, are combined again, and generate a constructive interference pattern. If the intensity of light is measured and plotted as a function of the position of the movable mirror, the resultant graph is the Fourier transform of the intensity of light as a function of wavenumber.

In this study, FTIR spectra in the wavenumber range 500–4000 cm^{-1} were recorded using Nicolet iS5 (THERMO Electron Scientific Instruments LLC) as shown **Figure III.13(b)**. Samples for recording FTIR spectra were prepared by mixing a few mg of the nano-powders with KBr to make pellets.

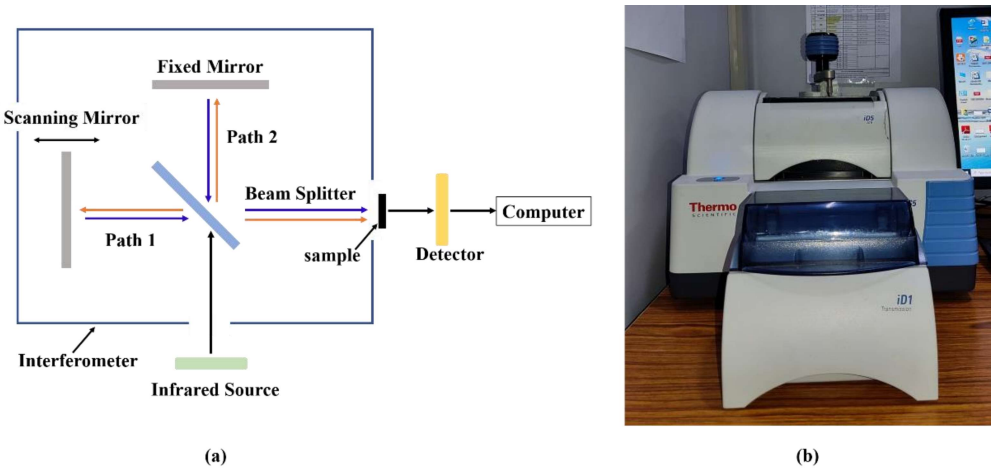

Figure III.13 (a) Schematic representation and (b) Instrumental picture of FT-IR spectrometer.

III.8.6 Differential Scanning Calorimetry

Differential Scanning Calorimetry (DSC) is a thermal analysis technique, it measures the heat flows related to transitions in material as a function of temperature and time in a controlled atmosphere. It is an useful technique to evaluate material properties such as glass transition temperature, melting, crystallization, specific heat capacity, curing process, oxidation behaviour, and thermal stability. DSC measurement offers quantitative and qualitative evidence related to physical and chemical changes that include endothermic or exothermic processes. The schematic representation of working of DSC is shown in **Figure III.14(a)**. Two types of DSCs are existing, a heat-flux DSC and a power-compensation DSC.

In present work, heat-flux DSC (**Figure III.14(b)**), (DSC)-60 Plus, M/s Shimadzu (Asia Pacific) Pte Ltd. was used. It measures the difference in temperature between a sample (T_s) and reference (T_r) heated at a programmed rate in a mutual furnace using thermocouples attached to the bottom of the sample holders. The temperature scanning was done at several scan rates (5, 10, 15, and 20 °C/min) in the temperature range of 40 °C to 550 °C under a nitrogen atmosphere for a powder of pure selenium, pure wz-CIS, and mixture of selenium and wz-CIS. And the phase transformation and crystallization were investigated.

Differential scanning calorimetry: Heat flow/ Specific heat capacity

$$\Delta H = C_p \Delta T \; or \; \frac{dH}{dt} = C_p \frac{dT}{dt} + thermal\ events$$

Where, C_p=specific heat(J/g°C), T=temperature (°C), H=heat (J), $\frac{dH}{dt}$ =Heat flow (J/min), $\frac{dT}{dt}$ =heating rate (°C/min)

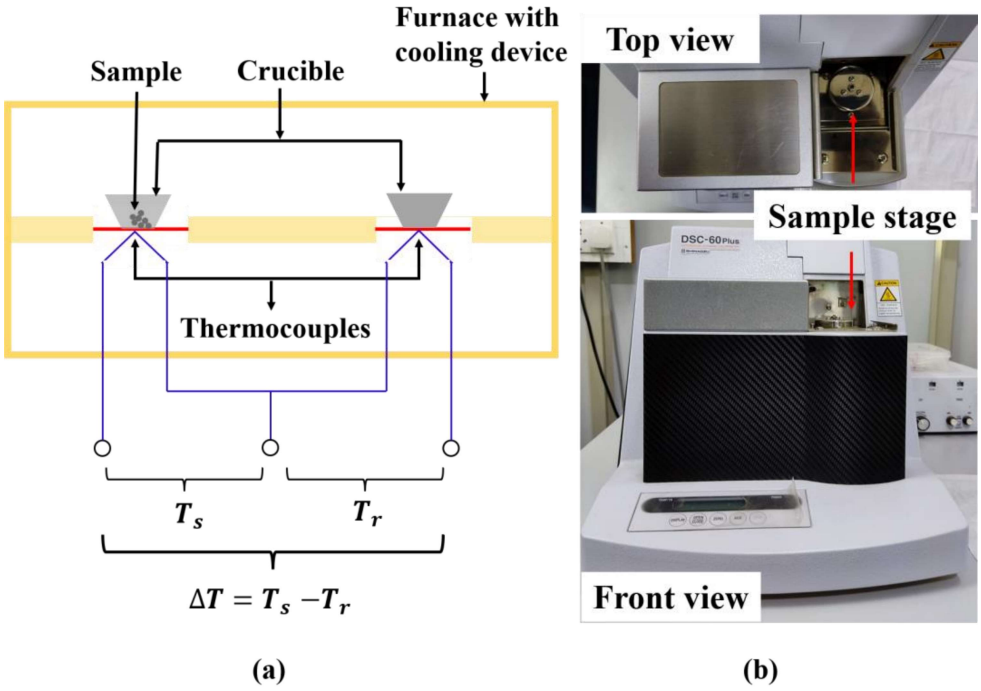

Figure III.14 (a) Schematic of heat-flux, (b) Actual photograph of Differential scanning calorimetry.

III.8.7 UV/Visible Spectroscopy

Ultraviolet (UV)-Visible Spectroscopy is one of the oldest and most widely used technique in spectroscopy, where wavelengths/energy of UV or visible light that are absorbed by or transmitted through the sample is measured in comparison to a reference blank sample. It generally operates in 280 to 1100 nm wavelength range. In present work, UV–visible/NIR spectrometer, JASCOV-770, USA was used to identify the bandgap of both nanoparticles and thin films of $Cu(In_xGa_{1-x})(S,Se)_2$.

Bandgap was determined by assuming that $Cu(In_xGa_{1-x})(S,Se)_2$, CdS, window layer is a direct bandgap material. In case of NPs, wurtzite $CuIn_xGa_{1-x}S_2$ NPs were dispersed in hexane and was placed in a cuvette (optical length = 10 mm).

III.8.8 Raman Spectroscopy

Raman Spectroscopy is a non-destructive chemical analysis technique, where scattered light is used to measure the vibrational energy modes of a sample. When monochromatic radiation falls upon a sample, it interacts with the sample. This interaction could be reflection, absorption or scattering in some manner. If the frequency (wavelength) of the scattered radiation is analysed, not only the incident radiation wavelength is seen (Rayleigh scattering) but also, a small amount of radiation that is scattered at some different wavelength (Stokes and Anti-Stokes Raman scattering). It is the change in wavelength of the scattered photon which provides the chemical and structural information. To check for possible binary compounds in the sprayed $Cu(In_xGa_{1-x})(S)_2$ and selenized $Cu(In_xGa_{1-x})(S,Se)_2$ samples, Raman spectra were recorded utilising micro-Raman spectrometer (Model UHTS300, WITec GMBH, Germany) with laser wavelength of 532 nm and laser power was kept at 10 mW during all the Raman measurements.

III.8.9 Solar Cell Characterization

A solar simulator is a controllable indoor test facility that provides illumination approximating natural light for the testing of wz-$CuIn_xGa_{1-x}S_2$ and ch-$CuIn_xGa_{1-x}(S,Se)_2$ solar cell devices. The solar simulator **(Figure III.15)** provides continuous illumination (xenon lamp) in time with an intensity of 100 mW/cm^2. The solar simulator (Model: #SS30AAA, Photo-Emission Tech., USA) is utilized

to measure the J/V curve using a Keithley 2450 source meter **(Figure III.15)**, along with the conversion efficiency, maximum power output, fill factor, series resistance, resistivity and shunt resistance of solar cells and other materials and devices. Voltage was scanned in the range of -1V to 1V, with voltage compliance of 1A. J-V curves were plotted by the parameter analyzer, and subsequent analysis was done with Microsoft Excel and Origin Labs software.

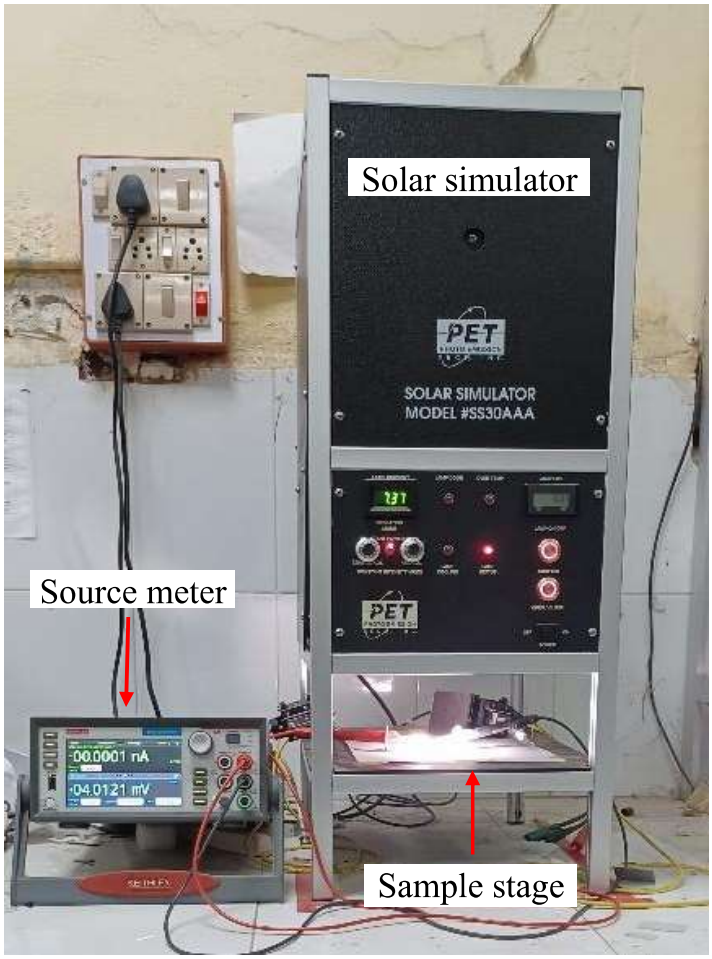

Figure III.15 Picture of a solar simulator for IV characteristic.